american physiological society

JNP JOURNAL OF NEUROPHYSIOLOGY

J Neurophysiol 128: 1617–1624, 2022.
First published November 16, 2022; doi:10.1152/jn.00340.2022

RESEARCH ARTICLE

Neuroscience of Disease

The brain landscape of the two-hit model of posttraumatic stress disorder

Lisa M. James,[1,2,3,4] Brian E. Engdahl,[1,2,4,5] Peka Christova,[1,2,4] Scott M. Lewis,[1,6] and Apostolos P. Georgopoulos[1,2,3,5,6]

[1]*The PTSD Research Group, Brain Sciences Center, Department of Veterans Affairs Health Care System, Minneapolis, Minnesota;* [2]*Department of Neuroscience, University of Minnesota Medical School, Minneapolis, Minnesota;* [3]*Department of Psychiatry, University of Minnesota Medical School, Minneapolis, Minnesota;* [4]*Center for Cognitive Sciences, University of Minnesota, Minneapolis, Minnesota;* [5]*Department of Psychology, University of Minnesota, Minneapolis, Minnesota; and* [6]*Department of Neurology, University of Minnesota Medical School, Minneapolis, Minnesota*

Abstract

The neurophysiological mechanisms underlying the development of posttraumatic stress disorder (PTSD) are poorly understood. Here we test a proposal that PTSD symptoms reflect fixed, highly correlated neural networks resulting from massive engagement of sensory inputs and the sequential involvement of those projections to limbic areas. Three-tesla functional magnetic resonance imaging (fMRI) data were acquired at rest in 15 veterans diagnosed with PTSD and 21 healthy control veterans from which zero-lag cross correlations between 50 brain areas (N = 1,225 pairs) were computed and analyzed. The brain areas were assigned to tiers based on the neurocircuitry of successively converging sensory pathways proposed by Jones and Powell (Jones EG, Powell TP. *Brain* 93: 793–820, 1970). The primary analyses assessed normalized proportional differences in cross correlation strength within and across tiers in veterans with PTSD and control veterans. Compared with control veterans, cross correlation strength was higher in veterans with PTSD, within and across tiers of areas involved in processing sensory inputs, and systematically increased from sensory processing areas to limbic areas. The functional relevance of this hypercorrelation was further documented by the finding that the severity of self-reported PTSD symptomatology was positively associated with higher neural correlations.

NEW & NOTEWORTHY The neurophysiological mechanisms underlying the development of PTSD are poorly understood. Here we document that massive engagement of sensory modalities during trauma exposure leads to fixed, hypercorrelated frontal, parietal, temporal, and limbic networks, reflecting the successive integration of salient sensory inputs along the framework of Jones and Powell.

functional magnetic resonance imaging; hypercorrelation; limbic; neural network; posttraumatic stress disorder

INTRODUCTION

Research over the last several decades has contributed to significant advancements in understanding the neurobiology of posttraumatic stress disorder (PTSD) from which several models have emerged. Dominant theories emphasize abnormal fear learning (1), exaggerated threat detection (2), deficient inhibitory control/emotion regulation (3), and/or altered contextual processing (4) as underlying PTSD. Indeed, as summarized in recent reviews (4–6), each of these theories has garnered substantial empirical support including evidence of alterations in several brain regions implicated in these processes, including the amygdala, anterior cingulate, insula, prefrontal cortex, thalamus, and hippocampus. These theories offer explanatory mechanisms for various signs and symptoms of PTSD, yet the mechanisms underlying the development of PTSD are not adequately accounted for in existing models and largely remain poorly understood. The focus of the present study is on neural network involvement in the development of PTSD.

PTSD is the only psychological disorder with known etiology, namely, exposure to a traumatic event. Typical examples of traumatic events include exposure to war, physical or

Correspondence: L. M. James (lmjames@umn.edu).
Submitted 5 August 2022 / Revised 25 October 2022 / Accepted 14 November 2022

sexual assault, accidents involving severe injury, and man-made or natural disasters (7). Although most people will not develop PTSD after exposure to such events (8), some may experience a host of impairing symptoms including reexperiencing of the event in the form of distressing involuntary memories, nightmares, or flashbacks, as well as distress related to trauma reminders and subsequent avoidance of such stimuli, hypervigilance, and exaggerated startle responses. Other symptoms including negative alterations in cognition or mood and other changes in arousal also occur but are not necessarily specific to PTSD (9).

It has long been established that traumatic memories are characterized by fragmented mental imprints of sensory aspects of traumatic experiences that are distinguished from ordinary memories by more prominent perceptual features (10). Thus, PTSD is first and foremost a sensory event. That is, traumatic events engage multiple sensory systems as they occur and, in the case of PTSD, that sensory information is stored and later manifested as reexperiencing symptoms. We postulate that the neurocircuitry associated with sensory pathways lies at the core of PTSD development.

In a groundbreaking paper, Jones and Powell (11) delineated the anatomical neurocircuitry involved in visual, auditory, and somatic pathways via painstaking lesion studies in the rhesus monkey. In general, they described an orderly sequence of projections from primary sensory areas to sensory association areas and then to sensory convergence areas, frontal and temporal poles, and ultimately limbic and basal ganglia regions. On the basis of this cortical organizational framework, coupled with evidence of neural network hypercorrelation in PTSD (12), we propose that massive engagement of sensory modalities during exposure to trauma leads to fixed, highly correlated downstream frontal, temporal, and ultimately limbic neural networks, reflecting encoding of salient sensory inputs corresponding to the pathways described by Jones and Powell (11). Furthermore, we postulate that PTSD is the involuntary outcome of behavioral decoding of those highly correlated neural ensembles manifested by the various PTSD symptoms.

In a recent paper (13) we proposed a model of PTSD development as the outcome of two hits: *1*) a background neuroinflammation and *2*) the occurrence of a traumatic event. We postulated the following stages in PTSD development: *1*) massive neural excitation initiated by the traumatic event and spread in the cortex and subcortical areas and *2*) intense glutamatergic synaptic activity, especially in the hippocampus, that is sustained by the soluble form of intercellular adhesion molecule ICAM-5 (sICAM-5), which is expressed during neuroinflammation, acting as local immunosuppressant (14, 15), but which also facilitates glutamatergic transmission and hippocampal excitability (16–18), thus leading to a vicious cycle of maintained excitation. Elevated expression of ICAM-5 has been observed only in people who developed PTSD after a traumatic event (19). The major region where ICAM-5 is expressed is the hippocampus, one of the limbic system structures involved in the final stages of sensory processing (11). In this study we assessed the cross correlation strength in veterans with PTSD compared with control veterans across sensory processing stages to characterize the sensory neurocircuitry associated with the development of PTSD.

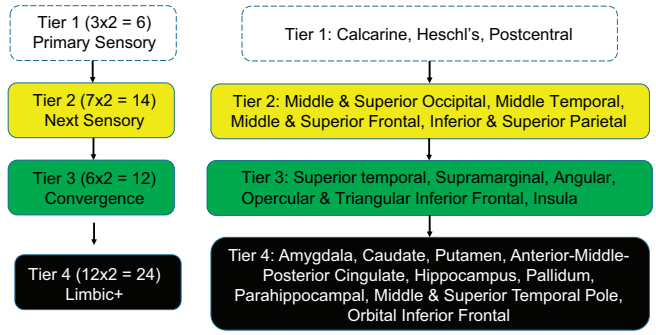

Figure 1. Schematic outline of the sequential processing of sensory input proposed by Jones and Powell (11).

MATERIALS AND METHODS

Participants

Fifteen veterans with a primary diagnosis of PTSD (13 men and 2 women) and 21 healthy control veterans (20 men and 1 woman) participated in the study. Diagnostic status was determined with the Clinician-Administered PTSD scale (20) and Structured Clinical Interview for DSM-IV-TR (21). The study protocol was approved by the Institutional Review Board at the Minneapolis VA Medical Center, subjects provided written informed consent before the study, and study procedures were performed in accordance with the institutional guidelines and regulations. Finally, the severity of PTSD symptoms was assessed with the Posttraumatic Stress Disorder Checklist for DSM-IV (PCL-IV) (22).

Data Acquisition

During resting-state functional magnetic resonance imaging (fMRI) acquisition, the participants were instructed to relax their mind, keep their eyes fixated ahead, and avoid moving and blinking. Imaging data were acquired with a 3-T MR scanner (Achieva; Philips Healthcare, Best, The Netherlands) with an eight-channel phased-array SENSitivity Encoding (SENSE) (23) SENSE-HEAD-8 head coil for reception. For each subject, a high-resolution T1-weighted anatomical image turbo field echo (TFE) was obtained [168 sagittal slices, repetition time (TR) = 8.0928 ms, echo time (TE) = 3.697 ms, voxel size = $0.9375 \times 0.9375 \times 1$ mm]. fMRI was acquired with fast field echo (FFE) transversal (axial) with whole brain coverage (TR = 2,000 ms, TE = 30 ms, flip angle = 90°, 40 axial slices per volume with slice scanning order

Table 1. *Descriptive statistics of data analyzed in the various tiers*

Tier	Number of Areas *N* (left and right)	Total Number of Pairs Possible $\frac{N(N-1)}{2}$	Minus the Number within [same − same] Tier	Actual Number of Pairs Analyzed
2–2	14	91	0	91
3–3	12	66	0	66
4–4	24	276	0	276
2–3	26	325	− (91 + 66)	= 168
2–4	38	703	− (91 + 276)	= 336
3–4	36	630	− (66 + 276)	= 288
All	50	1,225	0	1,225

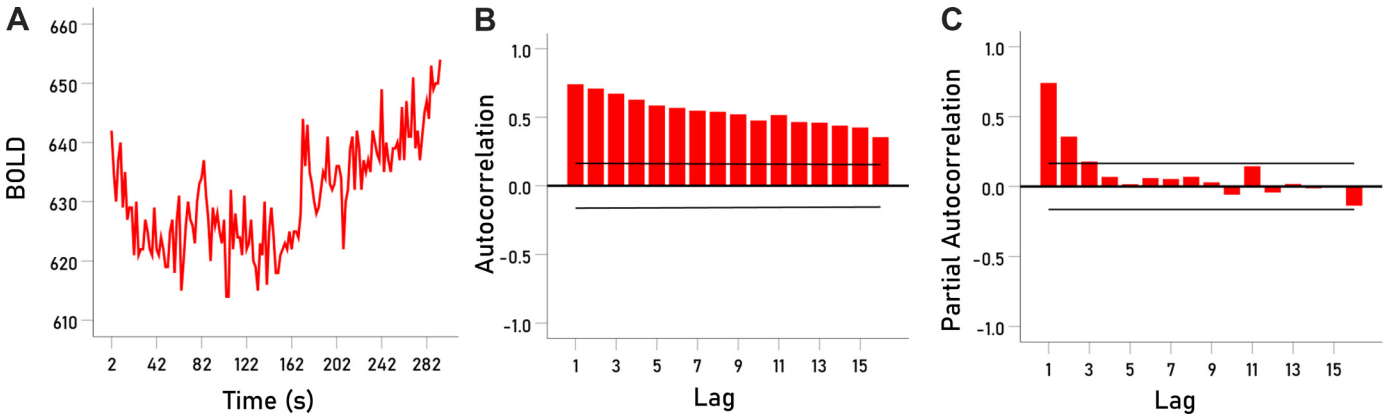

Figure 2. *A*: time course of raw blood oxygen level-dependent (BOLD) signal in a single voxel in the superior temporal gyrus of a posttraumatic stress disorder (PTSD) participant. *B* and *C*: note the nonstationary time course and associated high autocorrelations (*B*) and partial autocorrelations (*C*). Horizontal lines in *B* and *C* indicate 95% confidence intervals.

ascending, no interleaving, voxel size = $2.75 \times 2.75 \times 3.5$ mm). One hundred fifty consecutive whole brain fMRI volumes were obtained for 14 subjects and 203 volumes for 22 subjects, corresponding to 6,000 or 8,120 images, respectively. For all subjects, we used the first 150 volumes for further analyses.

The quality control of the acquired data included checking the results of each preprocessing step, ensuring the quality of the various alignments, and assessing head motion. The latter included analysis of the estimated motion parameter, provided by the output of Analysis of Functional NeuroImages (AFNI)'s robust realignment algorithm used for motion correction and alignment to a volume clean of artifacts, motion, and dropout. Specifically, participants with an estimated motion that exceeded a threshold less than half of the voxel size were excluded from further analysis. Next, blood oxygen level-dependent (BOLD) time series were prewhitened with autoregressive integrated moving average (ARIMA) (15,1,1), and white noise innovations (residuals) of the process were obtained (see *Data Preprocessing*).

Image Preprocessing

A 704-core high-performance Linux computer cluster (Rocks 5.4, CentOS 5.5) with MATLAB R2012 (64 bit), Analysis of Functional NeuroImages (AFNI), Surface Mapping (SUMA), and FreeSurfer (FS) 5.0.0 was used for data processing. All imaging data were analyzed with the AFNI software package (24). The first 3 volumes of each BOLD time series were discarded to allow for equilibrium magnetization. All remaining volumes were slice-time corrected and registered to the volume of the time series collected nearest in time to the acquisition of the anatomical scan. Motion correction was done with a Python script. Alignment of anatomical to functional MRI was done with a Python script with cost function local Pearson's correlation (25). Individual brains were then registered to the stereotactic space of Talairach and Tournoux (26) with a 12-parameter-affine registration. The transformation applied to the anatomical image was applied to the functional image together with resampling to the original voxel size. Cortical surface and subcortical brain areas, identified

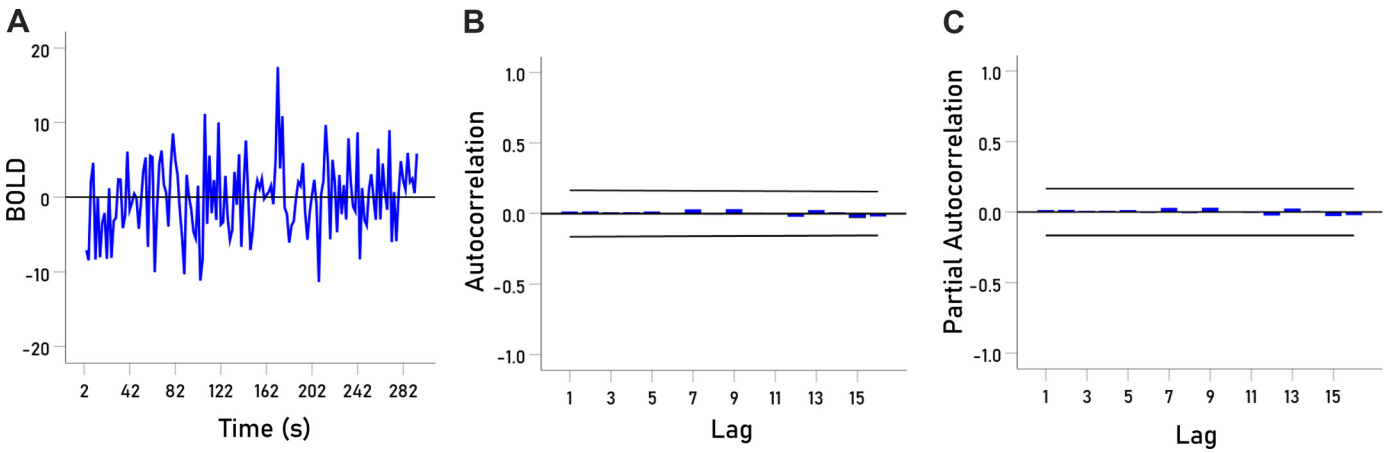

Figure 3. *A*: time course of the prewhitened blood oxygen level-dependent (BOLD) signal of the same voxel plotted in Fig. 2. The trace plots the innovations (residuals) following the application of an autoregressive integrated moving average (ARIMA) (15,1,1) model to the raw data in Fig. 2*A*. *B* and *C*: note the stationarity of the trace (centered at mean = 0) and the elimination of autocorrelations (*B*) and partial autocorrelations (*C*).

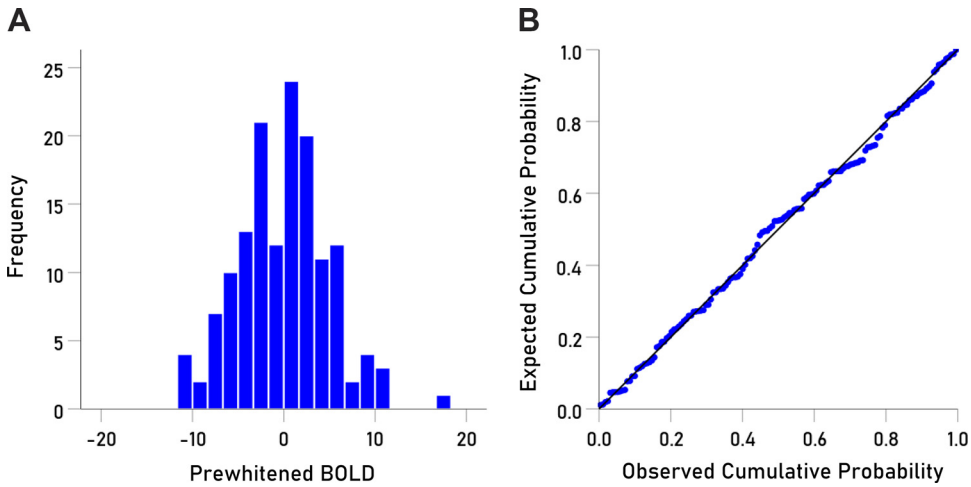

Figure 4. Histogram (*A*) and probability-probability (*B*) plots of the innovations of the prewhitened time course shown in Fig. 3*A*. Innovations are both independent (absence of autocorrelations, Fig. 3, *B* and *C*) and normally distributed (this figure). BOLD, blood oxygen level-dependent.

with FreeSurfer, were used as masks to extract the voxel time series. Data from 50 areas (25 in the left and 25 in the right hemisphere) could be assigned (to the best of our judgment) to successive sensory processing stages ("tiers") beyond the primary sensory cortices (visual, auditory, somatosensory) according to the cortical organization framework developed by Jones and Powell (11); these areas and tier assignments are shown in Fig. 1. In this study we analyzed data from *tiers 2*, *3*, and *4*, since we focused on the processing stages of sensory inputs and not on the primary sensory areas.

Data Preprocessing

First, the coefficient of variation of the BOLD time series of each voxel was calculated, and voxel series with a coefficient of variation >5% were eliminated from further analysis because of their likely proximity to large vessels (27). Next, single-voxel BOLD time series were prewhitened with a Box–Jenkins (15,1,1) autoregressive integrated moving average (ARIMA) model (28), as described in detail by Christova et al. (29). The resulting white noise innovations (residuals) were averaged across all the voxels within each area, which were then used to calculate zero-lag cross correlations between all possible pairs of the 50 areas used in these analyses; the total number of cross correlation values was $M = \frac{N(N-1)}{2} = \frac{50\times49}{2} = 1,225$. With respect to tiers (Fig. 1), there were 14 areas in *tier 2*, 12 areas in *tier 3*, and 24 areas in *tier 4*, yielding 91, 66, and 276 cross correlations in each tier, respectively. The numbers of pairs for each tier (*2–4*) are given in Table 1, which also shows the number of area pairs between tiers (*2–4*).

MR Data Analysis

First, the cross correlation values of r were Fisher z-transformed (30) to normalize their distribution:

$$r_z = \operatorname{arctanh}(r) = \frac{1}{2}\ln\left(\frac{1+r}{1-r}\right) \quad (1)$$

Next, for each pair of areas, the possible effect of age on r_z was assessed by running a linear regression of r_z on age. A statistically significant effect ($P < 0.05$) was found in 85/1,225 (6.9%) of cases, and these r_z values were adjusted for age (per area pair). Then, for each pair of areas, the normalized ratio (Q) of r_z between PTSD and control groups was computed:

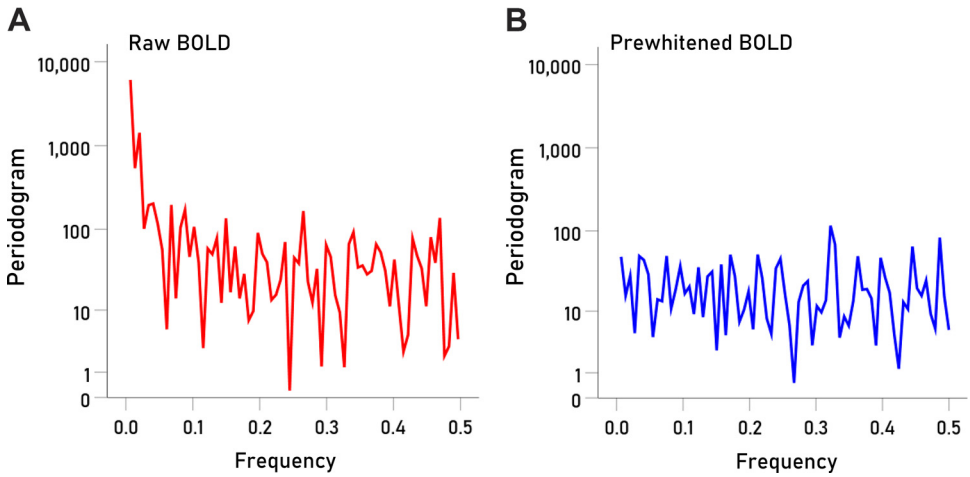

Figure 5. *A*: periodogram of the raw blood oxygen level-dependent (BOLD) time series (Fig. 2*A*). *B*: periodogram of the prewhitened BOLD time series (Fig. 3*A*). Note the presence and high power at low frequencies in *A* and their elimination in *B*. The periodogram in *B* is practically a "white" spectrum, hence the term "prewhitening."

Table 2. *Results of tests for counts of higher cross correlations in PTSD than control group*

Tier	Number of PTSD > Control	Total *N*	Proportion of PTSD > Control	Lower 95% CI	Higher 95% CI	*z*	*P* Value
2–2	64	91	0.703	0.603	0.787	3.88	<0.001
3–3	56	66	0.848	0.743	0.916	5.66	<0.001
4–4	216	276	0.783	0.730	0.827	9.39	<0.001
2–3	108	168	0.643	0.568	0.711	3.70	<0.001
2–4	246	336	0.732	0.682	0.777	8.51	<0.001
3–4	256	288	0.889	0.847	0.920	13.20	<0.001
All	946	1,225	0.772	0.748	0.795	19.06	<0.001

CI, confidence interval; PTSD, posttraumatic stress disorder.

$$Q = \frac{r_z^{\text{PTSD}} - r_z^{\text{Control}}}{|r_z^{\text{Control}}|} \times 100 \qquad (2)$$

The distribution of Q was skewed to the right, and therefore nonparametric statistics were used to analyze the data, including the calculation of the median and estimates of its variability. More specifically, variability estimates of the median Q (standard error and 95% confidence intervals) were obtained with a bootstrap procedure with the following parameters: number of samples = 1,000, Mersenne Twister random number generator, and bias-corrected and accelerated (BCa) confidence interval type. Testing for, and adjusting for, an age effect where needed was performed with Fortran (Intel Fortran Compiler, toolkit version: 2021.2.0). All other statistical analyses were performed with the IBM-SPSS statistical package (version 27). All P values reported are two sided.

RESULTS

Age

Participants in the PTSD group (age 48.8 ± 4.06 yr, mean ± SE, N = 15) were significantly younger than those in the control group (age 62.7 ± 1.65 yr, N = 21) ($P < 0.001$, independent samples t test).

PCL Scores

PCL scores were significantly higher in the PTSD group (57.00 ± 2.43, mean ± SE, N = 15) than in the control group (22.05 ± 1.37, N = 21) ($P < 0.001$, independent samples t test).

Prewhitening

Prewhitening was introduced by John Tukey (31–33) for estimating the association between two time series. Initially, it was applied in cross-spectral analysis, where the prewhitening yielded white noise innovations (residuals), the cross spectrum of which provided the true estimate of their association. Since the spectrum of white noise is flat across frequencies ("white"), the procedure was called "prewhitening." The requirement that time series be white noise for the correct estimate of their association to be obtained (34) applies to analyses in both the time (classical time series) and frequency (spectral) domains. Prewhitening in estimation of association between time series became a textbook procedure (28, 35).

As mentioned above, BOLD time series were prewhitened to remove trends and other within-series dependencies, an essential prerequisite for cross-correlating time series. Figure 2*A* shows an example of a raw BOLD time series from a single voxel in superior temporal gyrus of a PTSD patient; the presence of trends and other nonstationarities is obvious. This qualitative impression is documented by the high autocorrelations (Fig. 2*B*) and partial autocorrelations (Fig. 2*C*) of the series (well exceeding the 5% confidence intervals indicated by the 2 horizontal lines), both hallmarks of the presence of nonstationarities in the time series. Cross correlations between such nonstationary time series are spurious and typically high (36), as documented in various fields, including economics (37–39) and functional neuroimaging (29, 40–43). For valid cross correlations, the time series need to be stripped of internal dependencies and rendered stationary, nonautocorrelated, and, ideally, normally distributed. This is achieved by prewhitening the time series, which is commonly obtained by applying an ARIMA

Table 3. *Percent increase of median in PTSD r_z over Control in the various tiers and their combinations*

Tier	*N*	Median	SE	SNR	Lower 95% CI	Upper 95% CI
2–2	91	4.563	1.100	4.150	3.331	7.444
3–3	66	15.871	2.685	10.627	10.627	19.976
4–4	276	24.593	3.791	15.570	15.570	34.376
2–3	168	10.333	2.518	5.666	5.666	14.722
2–4	336	14.613	1.677	11.134	11.134	17.034
3–4	288	27.402	2.659	22.236	22.236	32.959
All	1,225	15.860	1.107	14.327	14.291	18.188

CI, bias-corrected accelerated (BCa) confidence interval (see MATERIALS AND METHODS); PTSD, posttraumatic stress disorder; r_z, z-transformed r; SE, standard error of the median; SNR, signal-to-noise ratio $\left(\frac{\text{Median}}{\text{SE}}\right)$.

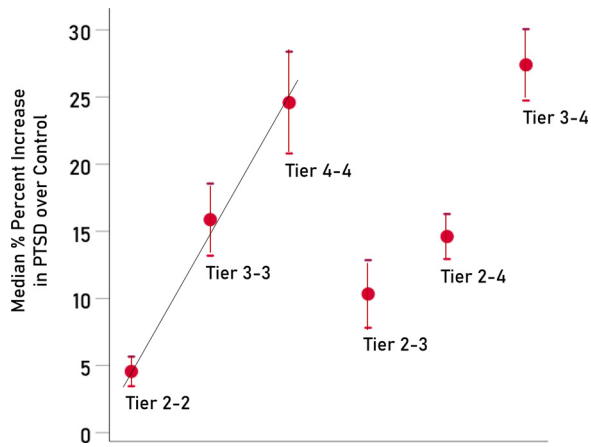

Figure 6. Median percent increases of z-transformed r (r_z) in posttraumatic stress disorder (PTSD) (over control) in the 3 area tiers and their combinations (Table 3). Vertical bars are ±SE.

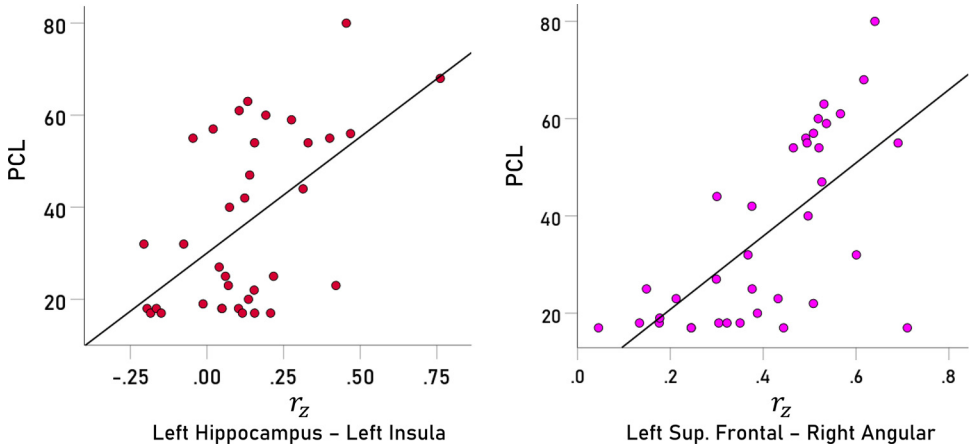

Figure 7. Posttraumatic Stress Disorder Checklist (PCL) values are potted against *z*-transformed *r* (r_z) for 2 pairs of areas, as indicated. *Left*: $r = 0.658$, $P = 0.000013$, $N = 36$. Right: $r = 0.611$, $P = 0.000074$, $N = 36$.

model and retaining the innovations (residuals) (28, 35). In previous work (29), we showed that an ARIMA (15,1,1) model (see MATERIALS AND METHODS) is sufficient for prewhitening typical fMRI BOLD series. Indeed, application of this model in the present study yielded innovations that were stationary (Fig. 3*A*), nonautocorrelated (i.e., independent; Fig. 3, *B* and *C*), and normally distributed (Fig. 4; Shapiro–Wilk test statistic = 0.991, degrees of freedom = 146, $P = 0.521$). The term "prewhitening" was coined by John Tukey (31–33) to denote the white spectrum resulting from this process. Indeed, this is illustrated in Fig. 5, where the periodogram (spectrum) of the raw BOLD time series (Fig. 5*A*), comprising high power at low frequencies, is contrasted with the practically "white" periodogram of the prewhitened BOLD time series (Fig. 5*B*), from which all low-frequency components have been eliminated.

Tiers: Increase in Cross Correlation Number and Strength in PTSD within and between Tiers

The numbers of normalized ratios (Q) analyzed in each tier group are given in Table 1. We found a large and highly statistically significant preponderance of increases in PTSD ($Q > 0$), overall, within and across tiers of areas, as shown in Table 2. We further quantified this effect and assessed its significance by calculating the median Q, its standard error (SE), and confidence intervals (derived by bootstrap, see MATERIALS AND METHODS), and a signal-to-noise ratio (SNR) of $\frac{\text{Median}}{\text{SE}}$ (a measure akin to the normal deviate z), The results are shown in Table 3 and plotted in Fig. 6. We found the following: *1*) There was an overall 15.86% increase of r_z in PTSD over control. *2*) Such an increase was observed for all within- and between-tiers combinations with SNR > 2 (a reasonable chance threshold). *3*) The magnitude of increase was systematically larger for higher tiers (median $Q[4–4]$ > median $Q[3–3]$ > median $Q[2–2]$) and their combinations (median $Q[3–4]$ > median $Q[2–4]$ > median $Q[2–3]$) (Fig. 6).

Table 4. *Detailed statistics of PCL vs. r_z for the various tiers and their combinations*

Tier	*N*	Median	SE	SNR	Lower 95% CI	Upper 95% CI
2–2	4	0.355	0.012	29.306	0.333	0.384
3–3	39	0.382	0.025	15.264	0.356	0.446
4–4	22	0.377	0.007	53.113	0.363	0.389
2–3	14	0.408	0.016	25.804	0.388	0.428
2–4	63	0.369	0.012	32.078	0.349	0.407
3–4	35	0.408	0.012	33.163	0.387	0.426
All	177	0.387	0.005	71.722	0.378	0.399

Median values are Pearson correlations. CI, bias-corrected accelerated (BCa) confidence interval (see MATERIALS AND METHODS); PCL, Posttraumatic Stress Disorder Checklist; r_z, *z*-transformed *r*; SE, standard error of the median; SNR, signal-to-noise ratio $\left(\frac{\text{Median}}{\text{SE}}\right)$.

Association of PCL Scores with r_z

We found a statistically significant association of PCL scores with r_z in 177/1,225 (14.4%) area pairs; of those, 174/177 (98.3%) were positive and 3/177 (1.7%) negative associations. Two examples are illustrated in Fig. 7. Median Pearson correlations between PCL and r_z were similar across tiers and their combinations (Table 4).

DISCUSSION

In the present study we evaluated the spatial distribution of correlated activity in PTSD within the framework of anatomical connectivity of multiple sensory inputs developed by Jones and Powell (11). In keeping with their scheme, we found progressively increasing cross correlations in PTSD, relative to control subjects, from secondary sensory areas (*tier 2*, first stage of sensory processing) to successive areas of multisensory convergence and ultimately limbic pathways.

PTSD Hypercorrelation

Generally, cross correlations between pairs of areas were characterized by hypercorrelation in the PTSD group relative to the control group and increased progressively along the sensory pathways. In a previous magnetoencephalography (MEG) study we demonstrated cortical hypercorrelation in PTSD relative to trauma-exposed healthy control subjects who, in contrast, were characterized by cortical decorrelation with trauma exposure (12). Decorrelation observed in control subjects was presumed to reflect neural network flexibility and underlie resilience in control subjects, whereas hypercorrelation in PTSD was deemed as reflecting a fixed state with limited neural network flexibility. Analyses of local cortical networks revealed that the right superior temporal pole and left temporal-parietal regions were among the most prominently decorrelated in control subjects. Neural

network differences in those same areas have been shown to provide highly accurate discrimination of PTSD from control subjects (44). Those regions are roughly akin to the convergence areas analyzed here. The present findings provide additional evidence of PTSD hypercorrelation and extend prior findings of cortical hypercorrelation to include subcortical regions not readily analyzed with MEG. Notably, the present findings documented associations between PTSD symptom severity and hypercorrelation involving relatively few (14%) pairs of areas, consistent with previous findings that a small number of neural correlations distinguish PTSD from control subjects (43–45).

PTSD Reflects Deficient Decorrelation

We postulate that the hard-wired plan initially elucidated by Jones and Powell (11) channels sensory inputs in specific ways such that intense and simultaneous multisensory stimulation leads to spatially progressive hypercorrelation. In the case of PTSD, it seems that this hypercorrelated state becomes fixed after exposure to traumatic events and concomitant sensory engagement. We suspect that in healthy control subjects a similar pattern of spatially progressive hypercorrelation results from exposure to potentially traumatic events; however, in healthy people the network gradually reverts to the normal, uncorrelated state. Consequently, PTSD can be characterized by deficient decorrelation (12). Factors underlying the persistence of this hypercorrelated state in PTSD as well as potential interventions aimed at facilitating decorrelation are being investigated.

Two-Hit Model of PTSD

We have proposed a two-hit model of PTSD in which PTSD is postulated to develop as a result of trauma exposure in the context of background neuroinflammation (13). Essentially, the two-hit model of PTSD proposes that a traumatic event initiates massive neural excitation accompanied by intense glutamatergic synaptic activity that is facilitated by ICAM-5 resulting from neuroinflammation. The present findings suggest that hypercorrelation in the PTSD group documented here is the functional outcome of the two hits. Here we found progressive increases in hypercorrelation across sensory processing tiers culminating in the largest difference from control subjects observed in the limbic regions. Consistent with our findings, previous studies concluded that limbic hyperactivity (coupled with decreased frontal inhibition) is a distinguishing feature of PTSD (46). We show that the limbic system involvement characteristic of PTSD reflects the progression of sensory processing pathways (11) resulting from trauma exposure in vulnerable individuals. This coupling of sensory processing pathways with limbic areas involved in emotional aspects of traumatic experiences and memory formation may reflect a brain mechanism underlying the characteristic symptoms of PTSD. Taken together, the present findings provide a compelling characterization of the brain landscape of PTSD development.

Limitations

The present study provides a novel contribution by evaluating neural network involvement in the development of PTSD. Nonetheless, several limitations must be considered. First, the sample is relatively small; thus, future studies with larger samples will be useful to evaluate replicability of the present findings. Along those lines, the sample size precluded evaluation of the influence of potential moderating variables including sex or trauma type. PTSD neural signatures have been shown to differ in men and women and for different types of trauma (45, 47, 48); however, the general progression of hypercorrelation along sensory pathways documented here is expected to reflect a fundamental mechanism of PTSD. As such, we do not expect the general pattern of progressively increased hypercorrelation across tiers of sensory pathways to differ by sex or trauma type, although that remains to be investigated.

GRANTS

This work was supported by Service-Directed Research Grant 3105 from the US Department of Veterans Affairs and the University of Minnesota (the American Legion Brain Sciences Chair, the William L. Anderson Chair in PTSD Research, the Anita Kunin Chair in Women's Healthy Brain Aging).

DISCLAIMERS

The sponsors had no role in the current study design, analysis, or interpretation, or in the writing of this paper. The contents do not represent the views of the US Department of Veterans Affairs or the United States Government.

DISCLOSURES

No conflicts of interest, financial or otherwise, are declared by the authors.

AUTHOR CONTRIBUTIONS

A.P.G. conceived and designed research; L.M.J. performed experiments; L.M.J., P.C., and A.P.G. analyzed data; L.M.J. and A.P.G. interpreted results of experiments; A.P.G. prepared figures; L.M.J. and A.P.G. drafted manuscript; L.M.J., B.E.E., P.C., S.M.L., and A.P.G. edited and revised manuscript; L.M.J., B.E.E., P.C., S.M.L., and A.P.G. approved final version of manuscript.

REFERENCES

1. **Jovanovic T**, **Kazama A**, **Bachevalier J**, **Davis M.** Impaired safety signal learning may be a biomarker of PTSD. *Neuropharmacology* 62: 695–704, 2012. doi:10.1016/j.neuropharm.2011.02.023.
2. **Buckley TC**, **Blanchard EB**, **Neill WT.** Information processing and PTSD: a review of the empirical literature. *Clin Psychol Rev* 20: 1041–1065, 2000. doi:10.1016/S0272-7358(99)00030-6.
3. **Falconer E**, **Bryant R**, **Felmingham KL**, **Kemp AH**, **Gordon E**, **Peduto A**, **Olivieri G**, **Williams LM.** The neural networks of inhibitory control in posttraumatic stress disorder. *J Psychiatry Neurosci* 33: 413–422, 2008.
4. **Liberzon I**, **Abelson TL.** Context processing and the neurobiology of PTSD. *Neuron* 92: 14–30, 2016. doi:10.1016/j.neuron.2016.09.039.
5. **Felmingham KL.** The neurobiology of posttraumatic stress disorder: recent advances and clinical implications. *Austral Clin Psychol* 3: 1742, 2018.
6. **van Elzakker MB**, **Staples-Bradley LK**, **Shin LM.** The neurocircuitry of fear and PTSD. In: *Sleep and Combat-Related Post Traumatic Stress Disorder*, edited by Vermetten E, Germain A, Neylan T. New York: Springer-Verlag, 2018.
7. **American Psychiatric Association.** *Diagnostic and Statistical Manual of Mental Disorders* (5th ed.). Washington, DC: American Psychiatric Publishing, 2013.

8. **Kessler RC**, **Sonnega A**, **Bromet E**, **Hughes M**, **Nelson CB.** Posttraumatic stress disorder in the National Comorbidity Survey. *Arch Gen Psychiatry* 52: 1048–1060, 1995. doi:10.1001/archpsyc.1995.03950240066012.
9. **Simms LJ**, **Watson D**, **Doebbeling BN.** Confirmatory factor analyses of posttraumatic stress symptoms in deployed and nondeployed veterans of the Gulf War. *J Abnorm Psychol* 111: 637–647, 2002. doi:10.1037//0021-843x.111.4.637.
10. **Van der Kolk BA**, **Fisler R.** Dissociation and the fragmentary nature of traumatic memories: Overview and exploratory study. *J Trauma Stress* 8: 505–525, 1995. doi:10.1007/BF02102887.
11. **Jones EG**, **Powell TP.** An anatomical study of converging sensory pathways within the cerebral cortex of the monkey. *Brain* 93: 793–820, 1970. doi:10.1093/brain/93.4.793.
12. **James LM**, **Engdahl BE**, **Leuthold AC**, **Lewis SM**, **Van Kampen E**, **Georgopoulos AP.** Neural network modulation by trauma as a marker of resilience: differences between veterans with posttraumatic stress disorder and resilient controls. *JAMA Psychiatry* 70: 410–418, 2013. doi:10.1001/jamapsychiatry.2013.878.
13. **Georgopoulos AP**, **James LM**, **Christova P**, **Engdahl BE.** A two-hit model of the biological origin of posttraumatic stress disorder (PTSD). *J Ment Health Clin Psychol* 2: 9–14, 2018.
14. **Gahmberg CG**, **Tian L**, **Ning L**, **Nyman-Huttunen H.** ICAM-5—a novel two-facetted adhesion molecule in the mammalian brain. *Immunol Lett* 117: 131–135, 2008. doi:10.1016/j.imlet.2008.02.004.
15. **Yang H.** Structure, expression, and function of ICAM-5. *Comp Funct Genomics* 2012: 368938, 2012. doi:10.1155/2012/368938.
16. **Niedringhaus M**, **Chen X**, **Dzakpasu R**, **Conant K.** MMPs and soluble ICAM-5 increase neuronal excitability within in vitro networks of hippocampal neurons. *PLoS One* 7: e42631, 2012. doi:10.1371/journal.pone.0042631.
17. **Lonskaya I**, **Partridge J**, **Lalchandani RR**, **Chung A**, **Lee T**, **Vicini S**, **Hoe HS**, **Lim ST**, **Conant K.** Soluble ICAM-5, a product of activity dependent proteolysis, increases mEPSC frequency and dendritic expression of GluA1. *PLoS One* 8: e69136, 2013. doi:10.1371/journal.pone.0069136.
18. **Tian L**, **Stefanidakis M**, **Ning L**, **Van Lint P**, **Nyman-Huttunen H**, **Libert C**, **Itohara S**, **Mishina M**, **Rauvala H**, **Gahmberg CG.** Activation of NMDA receptors promotes dendritic spine development through MMP-mediated ICAM-5 cleavage. *J Cell Biol* 178: 687–700, 2007. doi:10.1083/jcb.200612097.
19. **Wingo A**, **Daskalakis N**, **Galatzer-Levy I**, **Richholt R**, **Michopoulos V**, **Lori A**, **Guffanti G**, **Rothbaum B**, **Jovanovic T**, **Myers A**, **Huentelman M**, **Nemeroff C**, **Ressler K.** Transcriptome-wide analysis identifies ICAM5 differentially expressed in chronic PTSD symptoms versus resiliency post trauma exposure in a longitudinal study (Abstract). *Biol Psychiatry* 83: S91–S92, 2018. doi:10.1016/j.biopsych.2018.02.247.
20. **Blake DD**, **Weathers FW**, **Nagy LM**, **Kaloupek DG**, **Gusman FD**, **Charney DS**, **Keane TM.** The development of a clinician administered PTSD scale. *J Trauma Stress* 8: 75–90, 1995. doi:10.1007/BF02105408.
21. **First MB**, **Spitzer RL**, **Gibbon M**, **Williams JB.** *Structured Clinical Interview for DSM-IV-TR Axis I Disorders, Research Version, Nonpatient Edition (SCID-I/NP)*. New York: Biometrics Research, New York State Psychiatric Institute, 2002.
22. **Bliese PD**, **Wright KM**, **Adler AB**, **Cabrera O**, **Castro CA**, **Hoge CW.** Validating the Primary Care Posttraumatic Stress Disorder Screen and the Posttraumatic Stress Disorder Checklist with soldiers returning from combat. *J Consult Clin Psychol* 76: 272–281, 2008. doi:10.1037/0022-006X.76.2.272.
23. **Pruessmann KP**, **Weiger M**, **Scheidegger MB**, **Boesiger P.** SENSE: sensitivity encoding for fast MRI. *Magn Reson Med* 42: 952–962, 1999. doi:10.1002/(SICI)1522-2594(199911)42:5<952::AID-MRM16>3.0.CO;2-S.
24. **Cox RW.** AFNI: software for analysis and visualization of functional magnetic resonance neuroimages. *Comput Biomed Res* 29: 162–173, 1996. doi:10.1006/cbmr.1996.0014.
25. **Saad ZS**, **Glen DR**, **Chen G**, **Beauchamp MS**, **Desai R**, **Cox RW.** A new method for improving functional-to-structural MRI alignment using local Pearson correlation. *Neuroimage* 44: 839–848, 2009. doi:10.1016/j.neuroimage.2008.09.037.
26. **Talairach J**, **Tournoux P.** *Co-planar Stereotaxic Atlas of the Human Brain*. New York: Thieme, 1988.
27. **Kim SG**, **Hendrich K**, **Hu X**, **Merkle H**, **Uğurbil K.** Potential pitfalls of functional MRI using conventional gradient-recalled echo techniques. *NMR Biomed* 7: 69–74, 1994. doi:10.1002/nbm.1940070111.
28. **Box GE**, **Jenkins GM.** *Time Series Analysis: Forecasting and Control*. San Francisco, CA: Holden-Day, 1970.
29. **Christova P**, **Lewis SM**, **Jerde TA**, **Lynch JK**, **Georgopoulos AP.** True associations between resting fMRI time series based on innovations. *J Neural Eng* 8: 046025, 2011. doi:10.1088/1741-2560/8/4/046025.
30. **Fisher RA.** *Statistical Methods for Research Workers*. New York: Hafner, 1958.
31. **Press H**, **Tukey JW.** Power spectral methods of analysis and their application to problems in airplane dynamics. In: *Flight Test Manual*. Brussels: NATO Advisory Group for Aeronautical Research and Development, 1956, p. 1–41.
32. **Blackman RB**, **Tukey JW.** *The Measurement of Power Spectra from the Point of View of Communications Engineering*. New York: Dover, 1959.
33. **Brillinger DR.** John W. Tukey's work on time series and spectrum analysis. *Ann Stat* 30: 1595–1618, 2002.
34. **Priestley MB.** Fitting relationships between time series. *Bull Inst Int Stat* 38: 1–27, 1971.
35. **Priestley MB.** *Spectral Analysis and Time Series*. San Diego, CA: Academic, 1981.
36. **Yule GU.** Why do we sometimes get nonsense-correlations between time-series?—A study in sampling and the nature of time-series. *J R Stat Soc* 89: 1–63, 1926. doi:10.2307/2341482.
37. **Granger CW**, **Hatanaka M.** *Spectral Analysis of Economic Time Series*. Princeton, NJ: Princeton University Press, 1964.
38. **Granger CW**, **Newbold P.** Spurious regressions in econometrics. *J Econom* 2: 111–120, 1974. doi:10.1016/0304-4076(74)90034-7.
39. **Granger CW**, **Newbold P.** *Forecasting Economic Time Series*. New York: Academic, 1977.
40. **Tagaris GA**, **Richter W**, **Kim SG**, **Georgopoulos AP.** Box-Jenkins intervention analysis of functional magnetic resonance imaging data. *Neurosci Res* 27: 289–294, 1997. doi:10.1016/s0168-0102(97)01154-1.
41. **Locascio JJ**, **Jennings PJ**, **Moore CI**, **Corkin S.** Time series analysis in the time domain and resampling methods for studies of functional magnetic resonance brain imaging. *Hum Brain Mapp* 5: 168–193, 1997. doi:10.1002/(SICI)1097-0193(1997)5:3<168::AID-HBM3>3.0.CO;2-1.
42. **Leuthold AC**, **Langheim FJ**, **Lewis SM**, **Georgopoulos AP.** Time series analysis of magnetoencephalographic (MEG) data during copying. *Exp Brain Res* 164: 411–422, 2005. doi:10.1007/s00221-005-2259-0.
43. **Christova P**, **James LM**, **Engdahl BE**, **Lewis SM**, **Georgopoulos AP.** Diagnosis of posttraumatic stress disorder (PTSD) based on correlations of prewhitened fMRI data: outcomes and areas involved. *Exp Brain Res* 233: 2695–2705, 2015. doi:10.1007/s00221-015-4339-0.
44. **Engdahl B**, **Leuthold AC**, **Tan HM**, **Lewis SM**, **Winskowski AM**, **Dikel TN**, **Georgopoulos AP.** Post-traumatic stress disorder: a right temporal lobe syndrome? *J Neural Eng* 7: 066005, 2010. doi:10.1088/1741-2560/7/6/066005.
45. **James LM**, **Enghdal BE**, **Leuthold AC**, **Georgopoulos AP.** Classification of trauma-related outcomes in US veterans using magnetoencephalography (MEG). *J Neurol Neuromedicine* 6: 13–20, 2021. doi:10.29245/2572.942X/2021/1.1279.
46. **Etkin A**, **Wager TD.** Functional neuroimaging of anxiety: a meta-analysis of emotional processing in PTSD, social anxiety disorder, and specific phobia. *Am J Psychiatry* 164: 1476–1488, 2007. doi:10.1176/appi.ajp.2007.07030504.
47. **James LM**, **Leuthold AF**, **Georgopoulos AP.** Classification of posttraumatic stress disorder and related outcomes in women veterans using magnetoencephalography. *Exp Brain Res* 240: 1117–1125, 2022. doi:10.1007/s00221-022-06320-y.
48. **James LM**, **Leuthold AF**, **Georgopoulos AP.** MEG neural signature of sexual trauma in women veterans with PTSD. *Exp Brain Res* 240: 2135–2142, 2022. doi:10.1007/s00221-022-06405-8.